Molecular Dynamics Investigation of Structure and Transport in the $K_2O-2SiO_2$ System Using a Partial Charge Based Model Potential†

S. Balasubramanian‡ and K. J. Rao*

Solid State and Structural Chemistry Unit, Indian Institute of Science, Bangalore 560012, India

Received: May 12, 1994; In Final Form: August 9, 1994®

Potassium disilicate glass and melt have been investigated by using a new partial charge based potential model in which nonbridging oxygens are differentiated from bridging oxygens by their charges. The model reproduces the structural data pertaining to the coordination polyhedra around potassium and the various bond angle distributions excellently. The dynamics of the glass has been studied by using space and time correlation functions. It is found that K ions migrate by a diffusive mechanism in the melt and by hops below the glass transition temperature. They are also found to migrate largely through nonbridging oxygen-rich sites in the silicate matrix, thus providing support to the predictions of the modified random network model.

Introduction

The local environment around alkali cations in oxide glasses has been of considerable interest for a long time.[1,2] While lithium ions tend to coordinate to four oxygen atoms in a tetrahedral geometry, sodium ions tend to be five coordinated in a trigonal biprismatic geometry.[3] It is widely believed that potassium ions prefer to occupy octahedral sites.[4] Structural studies of alkali silicate glasses are important *per se* as well as to understand the structural factors contributing to electrical conductivity.[4,5] It is found that the activation energy for conductivity (E_a) in these glasses decreases drastically from >1.6 eV at low alkali concentrations to about 0.6 eV at around 15 mol % of alkali oxide, and above 15 mol % alkali oxide, it decreases very little when the alkali oxide concentration is increased up to 40 mol %.[4] The Haven ratio (the ratio of the tracer diffusion coefficient to that obtained from electrical conductivity) decreases from around 1 in silicates with low alkali concentration to around 0.4 in disilicate glasses.[5] This leads to the obvious conclusion that at low alkali concentrations, migrations are largely uncorrelated, while it is not so at higher concentrations. The exact manner of alkali ion transport has been the subject of several conjectures.[6] Recently Greaves[3] has suggested that specific conduction pathways are followed by the migrating alkali ions. The pathways reach their percolation thresholds after 15 mol % of alkali oxide. These pathways have also been considered to be largely one-dimensional and rich in nonbridging oxygens (NBO). The latter part of this assumption stems basically from the EXAFS results in which it was found that the number of NBOs around alkali ions is larger than that of bridging oxygens (BO). These suggestions are, as yet, unverified. In addition, earlier molecular dynamics results of Soules[7] and Angell[8,9] have suggested that the alkali ion motion is characterized by 'jumps' from site to site in the silicate matrix. Greaves has combined these suggestions in his modified random network (MRN) model,[3] and the principal assumptions of this model remain largely untested. Further, recent electrical conductivity studies[10] have revealed that, for alkali concentrations below the disilicate composition, the migration barrier is the rate-controlling step in the transport process of alkali ions. But for alkali concentrations above 33 mol %, it is the M−O bond breaking energy (M denotes alkali) which determines the transport so much so that, at these compositions, lithium has been found to have a higher activation energy than a much bigger caesium ion. It has also been observed that at the disilicate composition, the activation energy for conduction is independent of the type of alkali ion.

We therefore feel that it is very important to examine the details of alkali ion motion in alkali silicate glasses using the molecular dynamics method. In order to do that, it is an essential first step to use or devise an appropriate potential which can distinguish unambiguously the NBO's from the BO's. These potentials have to simultaneously reproduce other known static and dynamical features of silicate glasses. The second step is to choose a composition that provides a reasonable abundance of NBOs. This and perhaps a not so critical step is the choice of the alkali silicate. Keeping the above requirements in view, we have now performed a detailed molecular dynamics study of potassium disilicate glass using an ionic potential based on the one devised by Tsuneyuki *et al.*[11] for pure SiO_2. The advantages of this potential are presented in the next section along with the computational procedures adopted by us. In subsequent sections, the results are presented and discussed, keeping in view the vindication of the model potential from known static and dynamical properties and the prime thrust of this work, namely, examining the structural and dynamical aspects suggested in the MRN model.

The Potential and the Computational Details

In a series of papers, Tsuneyuki, Tsukada, Aoki, and Matsui[11] have described a potential of interaction (hereafter referred to as the TTAM potential[12]) for SiO_2, based on self-consistent Hartree−Fock calculations on model clusters. Similar attempts have also been made recently by van Beest and co-workers.[13] The TTAM potential is based on pairwise interactions and the key feature of this potential model is that it employs partial charges on Si and O (all oxygens being bridging in silica) equal to +2.4 and −1.2, respectively, which are lower than their formal charges.

The TTAM potential has been successfully employed in modeling various solid-state phase transitions in SiO_2.[11] Calculated values of unit cell dimensions of various polymorphs have been accurate to within 5%, bulk properties like density and bulk modulus within 10% and enthalpies within 1% of experimental results. Recent lattice dynamics calculations[14] on

† Contribution No. 944 from the Solid State & Structural Chemistry Unit.

‡ Presently at the Department of Chemistry, University of Pennsylvania, Philadelphia, PA 19104.

® Abstract published in *Advance ACS Abstracts,* September 15, 1994.

0022-3654/94/2098-10871$04.50/0

TABLE 1: Potential Parameters for the MD Run[a]

pair	A_{ij}, 10^{-15} J	B_{ij}, 10^{10} m^{-1}	C_{ij}, 10^{-17} J Å^6
K−K	3.149	5.0	0.00152
K−NBO	0.6488	3.523	0.0
K−BO	0.6488	3.623	0.0
K−Si	35.7	7.518	0.0
NBO−NBO	0.28088	2.441	0.01
NBO−BO	0.28088	2.7	0.556
NBO−Si	1.6234	4.784	1.08
BO−BO	0.28088	2.841	3.456
BO−Si	1.6234	4.784	1.178
Si−Si	95710.0	15.15	0.0

[a] $q_K = 1.0$; $q_{NBO} = -1.6$; $q_{BO} = -1.2$; $q_{Si} = 2.4$.

various polymorphs of SiO_2 indicate that this potential reproduces fairly well the observed Raman and IR spectroscopic data. The structure and properties of SiO_2 glass have also been studied succesfully by using this potential.[15] In addition, high-pressure studies on liquid SiO_2[12] and pressure amorphization of quartz[16] have also been studied recently by using this potential.

It has long been known that addition of alkali oxide to silica creates nonbridging oxygens (NBO). O1s X-ray photoelectron spectroscopy (XPS) data show that the negative charge on an NBO is higher than that on a BO.[17] This feature of an NBO has not been explicitly considered in any of the simulations on alkali silicates so far. Only recently Alavi *et al.*[18] have proposed and successfully implemented a charge-transfer MD method which seems to reasonably reflect the nature of the dynamic redistribution of charges, but unfortunately the potential parameters for alkali silicates have not yet been fully refined in this formalism. In the absence of a direct method, a distance criterion based on Si−O bond length has been used so far to identify NBO's. Although this was to some extent reasonable, it invariably led to a lesser number of NBOs than that suggested by the chemical formula.[19,20] Such a drawback can be eliminated by the use of a model in which the BO's and NBO's are associated with appropriate fractional or partial charges instead of the formal charges. The TTAM potential provides an excellent framework for building of such distinction between BO's and NBO's. Thus in the TTAM model,[11] if one assumes a +1 charge for the alkali cation and uses the fact that 1 mol of alkali oxide creates two NBOs as noted in XPS studies,[21-23] one can calculate the charge to be associated with an NBO as follows: Consider a $xM_2O(1-x)SiO_2$ system where M denotes any alkali ion. The number of each species present along with their charges is shown below.

species	no.	charge
Si	$1-x$	+2.4
M	$2x$	+1.0
BO	$2-3x$	−1.2
NBO	$2x$	q_{NBO}

The requirement of overall charge neutrality of the system sets q_{NBO} equal to −1.6. These charges have been used by us in the TTAM potential,

$$V(r_{ij}) = \frac{q_i q_j e^2}{r_{ij}} + A_{ij}\exp(-B_{ij}r_{ij}) - \frac{C_{ij}}{r_{ij}^6}$$

The various parameters employed in the potential are listed in Table 1. The A_{ij}, B_{ij}, and C_{ij} parameters for BO and Si are the same as those used for SiO_2 by Tsuneyuki *et al.*[11] and also by Valle and Andersen.[15] The A_{ij} and B_{ij} values for K−K and NBO−NBO interactions were obtained by assuming the radius of K to be 1.46 Å and that of NBO to be 2.34 Å. (In the original TTAM model,[11] the radius of BO was taken to be 2.05 Å.) In earlier MD simulations[19,24] also, the same ionic radius of K has been employed. The other parameters in the simulation, B_{ij}, and C_{ij} were chosen by a trial and error procedure so as to reproduce some of the known structural features in the system such as K−O, K−K, and K−Si nearest-neighbour distances.[25]

TABLE 2: Summary of Static Structure Data Obtained from Pair Distribution Functions at 300 K

pair	1st peak position, Å	coord no.	cut-off for coord no., Å	2nd peak position, Å
K−K	3.325	5.99	4.55	6.825
K−NBO	2.65	4.24	3.625	5.175
K−BO	2.8	1.75	3.35	5.175
K−Si	3.6	6.32	4.925	6.65
NBO−NBO	2.825	0.78	3.2	3.95
NBO−BO	2.775	2.01	3.1	5.15
NBO−Si	1.575	1.03	2.45	4.35
BO−BO	2.575	6.7	3.7	4.95
BO−Si	1.625	1.89	2.4	4.075
Si−Si	3.15	2.90	3.6	4.35

Thus, our system consists of four species, namely, K, NBO, BO, and Si. The molecular dynamics simulation was performed on a system of 504 atoms (112 K, 112 NBO, 168 BO, and 112 Si) in the microcanonical ensemble. The initial configuration of the system was chosen randomly in a cubic box with a minimum interatomic separation of 1.5 Å. Experimentally known glass density (2.467 g/cm^3) was used to obtain the box length. Such a use of glass density at higher tempertures (particularly at 3500 K) is clearly inappropriate and hence we confine our discussion of the structure and dynamics of ions to lower temperatures only (less than 2500 K). It should be noted that the migration of potassium ions in the glass can always be expected to be accompanied by bond-breaking and bond-forming processes in the vicinity.[18,26,27] The preceding analysis does not address this dynamic restructuring of the network.

The equations of motion were integrated with a time step of 1 fs. The system was equilibrated for over 40 ps at 3500 K (T5), from which it was quenched to 2500 K (T4), 1500 K (T3), 700 K (T2), and 300 K (T1) with a quench rate of 0.1 K per timestep. At each of the above temperatures, coordinates and velocities were recorded every 10 fs for over 60 ps (at 1500 K, the averages were performed over 135 ps) after a sufficient equilibration period of 40 ps. These were then analyzed in terms of structural and temporal correlation functions.

Results and Discussion

Static Structure. *Pair Distribution Functions.* In Table 2, we present results on the static structure of the glass obtained from the respective pair distribution functions (pdf). Let us first consider the correlations between ions that form part of the network, namely, Si, NBO, and BO. The NBO−Si and BO−Si pdfs are shown in Figure 1. It is known that the nearest-neighbor distances in the glass are identical to those in the crystalline material.[2] In crystalline α-$Na_2Si_2O_5$, it is reported that the Si−NBO bond length is 1.578 Å, whereas the Si−BO bond length is 1.630 Å.[28] In our simulated glass, the Si−NBO bond length is 1.575 Å and the BO−Si bond length is 1.625 Å in very good agreement with experiments. Similarly, a somewhat shorter (by about 0.05 Å) Si−NBO bond length compared to Si−BO distance has been observed recently in *ab initio* molecular orbital calculations on $H_4Si_2O_7K_2$ clusters by Uchino *et al.*[29] and in the MD results of Alavi *et al.*[18] The coordination numbers for NBO−Si and BO−Si are found to be 1.04 and 1.9, respectively, and are in good agreement with the expected values (1.0 and 2.0, respectively). This indicates that the process of modification due to the addition of alkali oxide to the system

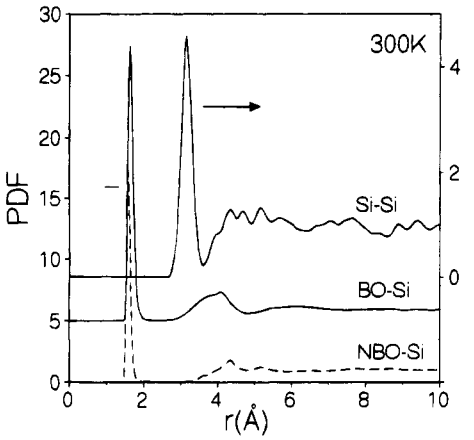

Figure 1. NBO–Si, BO–Si, and Si–Si pair distribution functions at 300 K. The first peak positions between the former two differ by about 0.05 Å.

visualized in traditional structural models is well reflected in the simulation. The inverse coordination number, i.e., Si–O (all oxygens are included), is around 3.88 at all temperatures and confirms that the integrity of the tetrahedra remains largely unaffected in the liquid state. The effect of modification is also reflected in the reduced Si–Si coordination number of 2.9 and the corresponding pdf is shown in Figure 1. The Si–Si nearest-neighbor distance is around 3.15 Å and matches well with the Si–Si distance obtained from neutron diffraction experiments.[25,30] This distance does not vary much with temperature while the coordination number increases from 2.9 at 300 K (in the glass) to around 3.3 at 3500 K (in the melt), which indicates closer packing of the tetrahedra at higher temperatures as expected from the melting behavior of SiO_2, which is like that of ice. For a disilicate glass, one expects the Si–Si coordination number to be 3.0 and hence this result can also be taken as additional support for the model.

We wish to emphasize that the present potential model is novel in the sense that NBOs are treated as separate entities. It involves a bit of empiricism since the number of NBO's has been fixed from the knowledge of composition. It would be interesting to examine if the predesignated NBO's are nonbridging by the distance criterion also. We have observed that at 300 K, nearly 88% of the NBO's are nonbridging by the distance criterion of Si–O bond length being 2.4 Å. Similarly, 87% of BO's indeed bridge two SiO_4 tetrahedra. Thus the present model reflects the essential static structural features of the alkali disilicate glass, including well-known structural consequences of the network modification process.

The distribution of NBO's in the glass can be obtained through ^{29}Si magic angle spinning nuclear magnetic resonance (MASNMR) experiments and expressed in terms of Q_n (n = 0–4) species ($Q \equiv$ Si and n is the number of BO's associated with Si; n varies from 0 to 4). By use of the data pertaining to the coordinates of all the atoms, the distribution of Q_n species can also be obtained in molecular dynamics simulations. The distribution of Q_n species obtained from our simulation is shown in Figure 2. It is clear that Q_3 dominates the distribution as has been observed in experiments.[31–33] The proportion of Q_4 species in our simulations is somewhat higher and can be attributed to the well-known disproportionation reaction:

$$2Q_3 = Q_4 + Q_2$$

In general, disproportionation reactions such as

$$2Q_m = Q_{m+1} + Q_{m-1}$$

have often been proposed to account for the existence of more

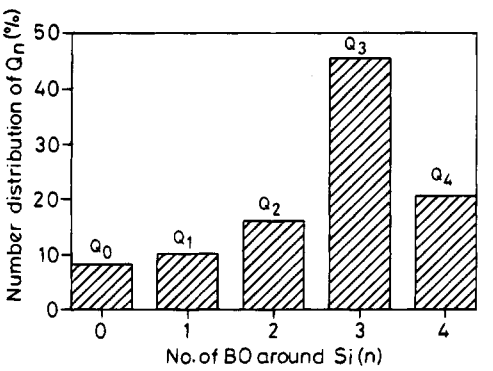

Figure 2. Histogram of Q_n species in the glass at 300 K. Q_n denotes a silicon coordinated to n BO's.

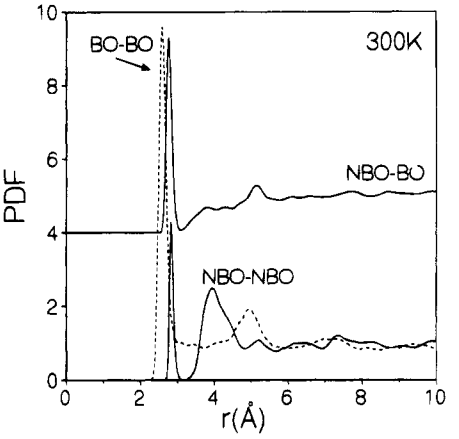

Figure 3. Various oxygen–oxygen pair distribution functions at room temperature.

resonances in the NMR spectrum than those suggested by the chemical composition.[34–36] Indeed in our simulations also, we observe around 16% of silicon atoms to be of Q_2 type. The experimental reports with regard to the exact quantity of each species is, to date, somewhat controversial. While Dupree *et al.*[35] observe only Q_3 species in the disilicate compositions, other workers including Selvaraj *et al.*[36] and Stebbins[32] observe a finite proportion of silicon atoms to be of Q_4 type. But Furukawa *et al.*[37] have observed a 950-cm^{-1} band in the Raman spectra of sodium disilicate glass, which they assign to the symmetric stretching of $Si-O^-$ bonds in species of Q_2 type. Hence, while the magnitude of Q_4 (or, in effect, Q_2) is not undisputed, various reports seem to agree upon the existence of species other than Q_3 in the disilicate glass. We believe that the larger amount of Q_4 present in our simulations could also be due to the high fictive temperatures inherent to any computer-simulated glass. This can also arise due to the inadequacy of the NBO–NBO interactions in the model, but this reason is less likely, because the NBO–NBO coordination number is found to be quite low (around 0.8, see later).

The various oxygen–oxygen pdfs are shown in Figure 3. The NBO–NBO coordination number is low (0.8). This may be attributed to the higher repulsive interaction between them. The BO–BO coordination number is around 6.7 and is somewhat higher than the BO–BO coordination number of 6 obtained for pure silica glass by using the same potential.[15] The NBO–BO coordination number is only around 2.0. The average oxygen–oxygen coordination number (ignoring the BO and NBO labels) in our work is found to be around 6.3.

In Figure 4, we present the K–NBO and K–BO pdfs. The first peak is indicative of the local environment around K and its position is in good agreement with experiments.[25,38] It is

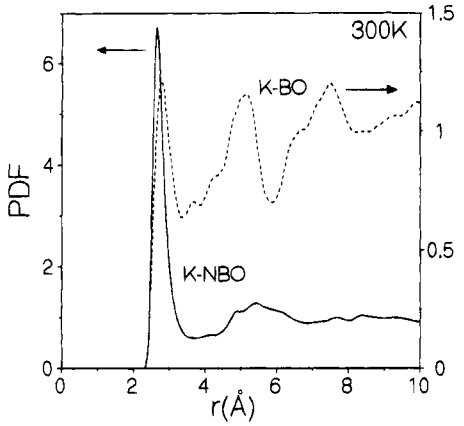

Figure 4. K−NBO and K−BO pair distribution functions in the glass.

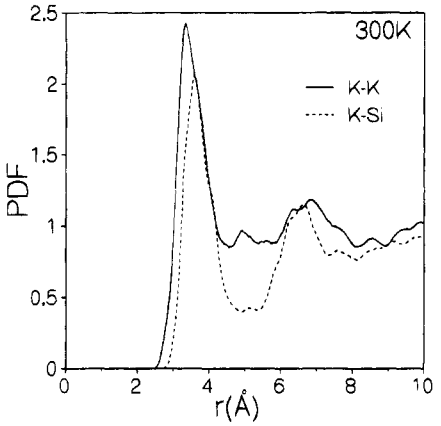

Figure 5. K−K and K−Si pair distribution functions at 300 K.

interesting to note the coordination numbers in both the cases. The K−NBO coordination number is around 4.25, while that of K−BO is ≈1.75. These data strongly support the MRN model of Greaves.[3] Vessal *et al.* in their MD simulations on mixed alkali silicate glasses also provided similar evidence, albeit indirect.[39] A similar observation was also made in simulations of mixed alkali silicate glasses[20] reported from this laboratory, in which a distance criterion was employed to identify NBO's. The present set of simulations provide a rather direct support in favor of the assumptions made in the MRN model. The fact that in a static average, the alkali ions are surrounded by more NBO's than BO's indicates that only sites with such high NBO coordination are likely to be involved during K^+ ion transport. This observation is substantiated by the dynamical data to be discussed later.

K−K distances are strongly correlated (Figure 5) and are observed at almost the same distances as in other studies.[40] It is worthwhile to note that the K−K coordination at room temperature is close to 6. Unfortunately, crystalline data on $K_2O-2SiO_2$ is not available but in the isostructural six-net structure of α-$Na_2Si_2O_5$, Na−Na coordination is 6.[41] Gaskell, through neutron scattering methods,[42] and Abramo *et al.*,[43] through MD calculations, have argued that the local structure in the glass is closely related to the crystalline analogue. Our results seem to support these arguments. It is interesting to consider in this context the K−Si pdf shown in Figure 5. The coordination number for the same is found to be around 6.3. When the K−O and the K−Si coordination numbers are considered together, it seems likely that the six oxygens (≈4.25 NBOs and 1.75 BOs) surrounding the K ion possibly belong to six different SiO_4 tetrahedra. We will discuss the geometrical dispositions of the oxygen ions around K ions later. A common feature of the pdfs considered so far is their dependence on

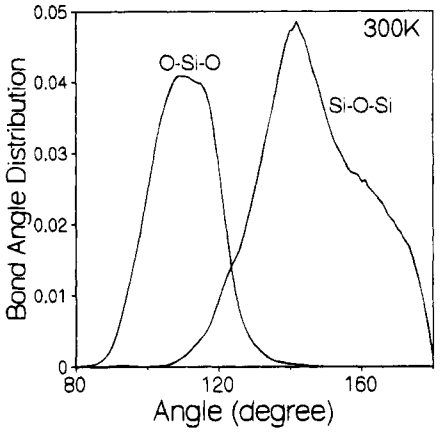

Figure 6. O−Si−O and Si−O−Si bond angle distributions in the glass at 300 K. The peak position for the angle at silicon is 109°, while that for oxygen is 143°.

temperature. As the temperature is increased, the pdfs start gaining intensity in the hard sphere region (distances much below the first peak), and the correlations tend to decrease in height and increase in width. These are purely manifestations of the increased kinetic energy at higher temperatures.

Bond Angle Distributions. The O−Si−O and Si−O−Si bond angle distributions are shown in Figure 6. We find that the angle at silicon is rather sharp with a single peak at around 109°, confirming the tetrahedral nature of the SiO_4 unit. The Si−O−Si bond angle distribution shown in Figure 6 has a sharp peak at around 143° with a HWHM of around 18°. This is in excellent agreement with recent two-dimensional ^{17}O dynamic angle spinning NMR data[44] of potassium disilicate glass where the Si−O−Si angle distribution was observed to be 143° with a HWHM of around 21°. Earlier MD results employing both two-body[24,20,45] as well as three-body potentials[39,46,47] have largely failed in accurately reproducing the bond angle distribution. The only other potential model which successfully reproduces both the bond angle distributions was developed by Vashishta *et al.*[48] employing three-body forces. The distribution from our study also exhibits a small hump at around 157°, which is likely to arise out of some BO's which are singly bonded to Si (around 13%). Since these BO−Si distances are smaller, they could lead to a higher-than-143° angle. In fact, in crystalline α-$Na_2Si_2O_5$, two Si-O-Si angles have been observed,[28] one at 138.9° and the other at 160°. Thus, a noteworthy feature of the TTAM potential[11] is the fact that it provides very satisfactory O-Si-O and Si-O-Si bond angle distributions, although it contains only pairwise interactions (there are no three-body terms as in the work of Feuston and Garofalini[46] and Vessal *et al.*[39]). It is well-known that the width of the bond angle distribution at oxygen is a direct measure of the disorder in the system. Hence the excellent agreement of the bond angle distribution obtained from the simulations with those obtained from experiments is a compelling support for the appropriateness of the model potential.

From the various pdfs, we had concluded earlier that, in general, a K ion is coordinated to around six oxygens (4.25 of NBO type and 1.75 of BO type). We observe from the O−K−O bond angle distribution (here O represents oxygens of both the types) at 300 K (Figure 7a) that this angle is predominantly 90°, with a smaller peak at 50°. The 90° angle indicates that potassium is likely to be present in an octahedral site surrounded by oxygens as envisaged by various workers.[26] The 50° angle arises mostly out of triplets of the type BO−K−BO (Figure 7a), where the BO−BO distance (2.6 Å) is shorter than the NBO−NBO distance (2.825 Å), whereas the

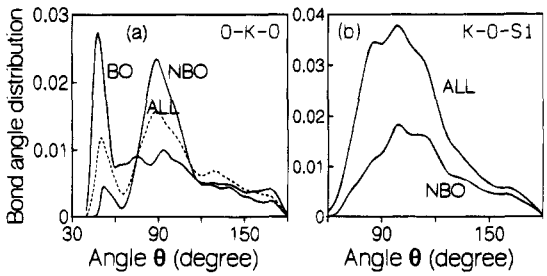

Figure 7. Bond angle distributions of (a) O−K−O and (b) K−O−Si in the glass at 300 K. The angle at potassium shows a peak at around 90°, denoting an octahedral environment for K ions. The small peak at 50° arises out of K ions in BO rich environments.

peak at around 90° comes from triplets of the type NBO−K−NBO. The K−O−Si angle distribution (Figure 7b) also shows a peak at around 90°, though the distribution is rather broad. This further supports the conclusion that each SiO_4 tetrahedron contributes one oxygen to the coordination octahedron around potassium.

Dynamics. Thus we note that the present potential model reproduces the known structural features of silicate glasses. More importantly, it was found that K^+ ions are present in oxygen octahedra consisting of larger number of NBOs (4.25) than just the stoichiometric average (2.4). This feature is an indirect support for the MRN model.[3] We have studied in detail the dynamics of the silicate network elements (Si, NBO, and BO) and the alkali cations in the glass in this background in order to understand the nature of transport of K ions in the silicate matrix. Toward this aim, we have calculated the various velocity correlation functions and their Fourier transforms, mean-squared displacement of the ions, and the van Hove correlation functions (the self part, VHS, and the distinct part, VHD), which provide detailed information on the migration processes. It has long been known that NBO's play an important role in the migration of alkali ions.[8,9] Hence we have studied individual migration processes of potassium ions to find out if there is unambiguous selectivity in their migration paths, i.e., whether they migrate preferentially through NBO rich channels. These data, in particular the VHS and VHD, are extremely sensitive to the length of the simulation runs. Hence we have calculated them for over a period of 135 ps at 1500 K, which is just below the T_g of the computer quenched glass, and for 65 ps at other temperatures.

Velocity Autocorrelation Functions. Figure 8a shows the small time behavior of the velocity autocorrelation function (VAF) of K ions at three temperatures. The negative dip in VAF denotes backscattering of potassium within the oxygen cage and it is fairly straightforward to understand that as the temperature is increased, the cage weakens, resulting in a less negative minimum in the VAF. The power spectrum (Fourier transform) of the VAF of K ions at 300 K is presented in Figure 8b. It exhibits a peak at 145 cm^{-1} with a HWHM of around 80 cm^{-1}. The peak position corresponds to the cage vibration frequency and is in very good agreement with the reported far-infrared spectrum.[49] We have also calculated the power spectra of the individual VAFs of the ions which are part of the network and the power spectrum of the VAF of the network considered as a whole.[50] The VAF of the network is defined as

$$C(t) = \frac{\langle \sum_i \vec{v}_i(t_0) \cdot \vec{v}_i(t_0 + t) \rangle}{\langle \sum_i \vec{v}_i(t_0) \cdot \vec{v}_i(t_0) \rangle}$$

where the index "i" runs over all the silicon, NBO and BO atoms.

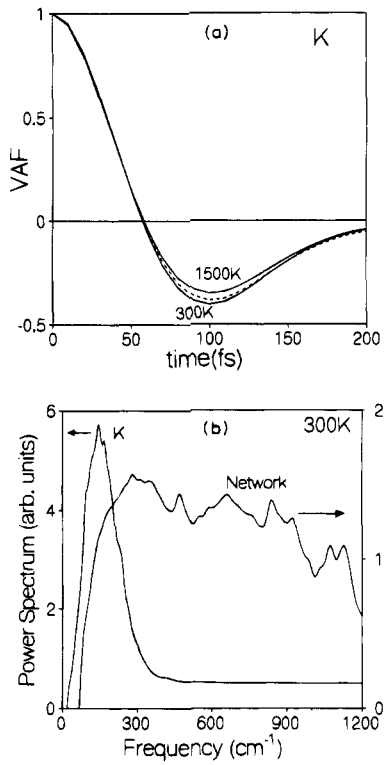

Figure 8. (a) Small time behavior of the velocity autocorrelation function of the potassium ions at three different temperatures. At 1500 K, the surrounding cage structure weakens relative to that at 300 K and hence the negative minimum becomes shallow. The dashed line is the behavior at 700 K. (b) Power spectra of K ions and the network considered as a whole at 300 K obtained as the Fourier transform of the respective velocity autocorrelation functions.

The power spectrum of the network considered as a whole is also presented in Figure 8b. It is clear that the network has three main features as observed in experiments.[51,52] These are broadly at 400, 800, and 1100 cm^{-1}. The low-frequency vibrations are ascribed to cation (Si) motion and bond rocking, where the oxygen vibrates in a direction perpendicular to the Si−O−Si plane; the 800-cm^{-1} peak is associated with symmetric stretching of bonds and bond bending modes, while the higher wavenumber features are ascribed to asymmetric stretching of Si−O bonds.[50] In particular, we would like to note that the transverse optic/longitudinal optic (TO/LO) vibrational mode splitting[48,52] at around 1100 cm^{-1} is observed clearly in our simulations. As in the present work, the vibrational density of states and the dynamic structure factor of silica calculated by using the TTAM potential has been recently studied.[53] The details of the various features in the vibrational density of states have been discussed in detail by Price and Carpenter[52] recently. We observe that the present model compares quite favorably with existing literature data.

Mean-Squared Displacements. While the local motion of various ions in the glass can be obtained by studying their VAF's, their long-range motion can be understood through a study of the mean-squared displacement (MSD) data. These are displayed for K ions in Figure 9 at 2500 and 1500 K. The diffusion coefficients (D) of all the ions obtained from the slope of the MSD curves are presented in Table 3. At any temperature, the diffusion coefficient values decrease in the order of $D_K > D_{NBO} > D_{BO} > D_{Si}$. This behavior is on expected lines.

It is widely known that NBO's are somewhat more mobile (being just one connected) than BO's. This is also reflected in the fact that NBO's contribute to a high-temperature (353 K) peak in internal friction experiments.[54] The diffusion coefficient

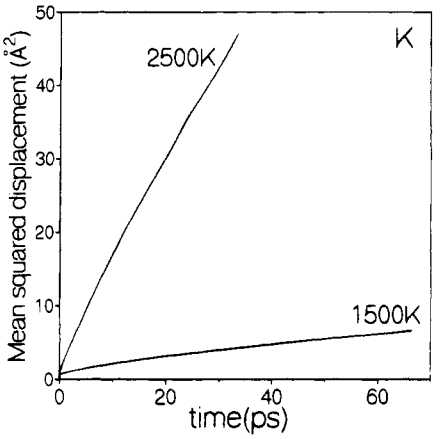

Figure 9. Mean-squared displacement data of potassium ions at 1500 and 2500 K plotted as a function of time.

TABLE 3: Diffusion Coefficients of Ions at Various Temperatures ($\times 10^{-5}$ cm²/s)

ion	1500 K	2500 K	3500 K
K	0.127	2.001	7.493
NBO	0.013	0.341	2.844
BO	0.008	0.285	3.250
Si	0.006	0.221	2.215

of K ions is around 2×10^{-5} cm²/s (typical liquid values) only at 2500 K. We feel that the system is somewhere near its T_g below this temperature. We have not performed the necessary analysis to exactly locate the T_g of the system, as that would require extended runs at more temperatures than what has been performed now. At 700 and 300 K, the mobilities of the ions are extremely small and thus their diffusion coefficients could not be measured accurately.

Self Part of van Hove Correlation Functions. The MSD provides the magnitude of the migration during transport. To understand the details of the transport process as a function of temperature, van Hove correlation functions are best suited.[19,20,55,56] These provide rich information on the nature of migration, particularly the length and time scales inherent to the transport process. Figure 10 shows $4\pi r^2 G_s(r,t)$ (VHS) data of K ions for five arbitrary times as a function of distance at 700, 1500, and 2500 K. The curve at 700 K does not change its position nor its shape for all the times. This denotes that the potassium ions are fairly immobile at this temperature, further confirming the result obtained through the mean-squared displacement data. The peak position is related to the Debye–Waller factor at this temperature.[56] At 1500 K, we find at small times a single peak structure. At higher times, a second peak develops at around 3.5 Å. The first peak at around 1 Å, which shifts to higher distances rather slowly, represents the K ions which are found in the same cage after a time t (the distance is less than half the diameter of an average cage). The fact that this shifts as a function of time toward higher distances coupled with the presence of a second peak indicates a finite slope in the corresponding MSD curve. The second peak clearly establishes the nature of the migration process, namely, hoplike events. If the process were simply diffusive, the minimum at around 2 Å would not be present. Such a feature has also been noticed and analyzed in detail by Barrat and Roux[56–58] in simulations of supercooled soft spheres just below T_g and in supercooled Lennard–Jones liquids by Wahnström.[59] It is worthwhile to note here that such hoplike events have been observed in lithium-conducting aluminosilicate glass ceramics recently using broad-band impedance spectroscopy.[60] The import of the VHS of K ions shown in Figure 10c is clear. At

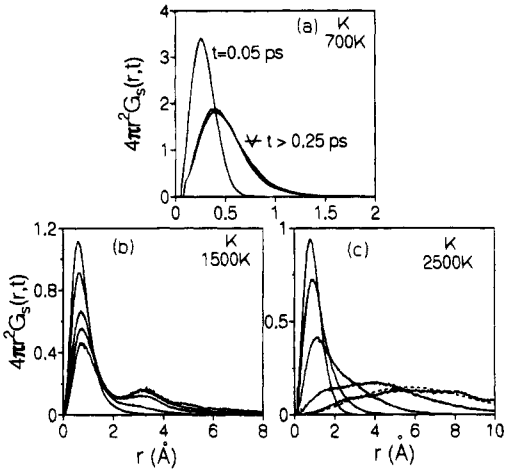

Figure 10. $4\pi r^2 G_s(r,t)$ plotted as a function of distance for the potassium ions at three temperatures for various times: (a) at 700 K; (b) at 1500 K. At the first peak position, curves correspond to the following times in decreasing order of height. Time in picoseconds: 1; 9; 40; 70; 110. The curves corresponding to times beyond 40 ps show a clear second peak at around 3.5 Å, denoting hop-like motion of the K ions. (c) At 2500 K. Time in picoseconds: 0.15; 0.5; 3; 16; 40. The fit of the hydrodynamic diffusion equation for $t = 40$ ps is shown as a dashed line.

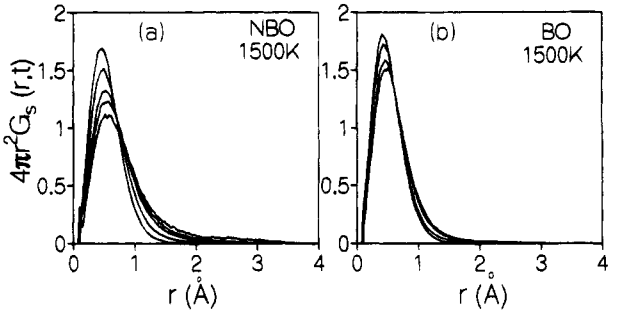

Figure 11. $4\pi r^2 G_s(r,t)$ plotted as a function of distance for the NBO and BO ions at 1500 K for various times: (a) NBO and (b) BO. At the first peak position, curves correspond to the following times in decreasing order of height. Time in picoseconds for all cases: 0.15; 1; 9; 20; 50.

this temperature (2500 K), the motion of K ions is fully diffusive and liquidlike, and there are no hops, at least at the level of the VHS function. The function fully relaxes by about 40 ps. The behavior at this time can be easily fitted to the hydrodynamic limit,

$$G_s(r,t) = \frac{1}{(4\pi Dt)^{3/2}} \exp\left(\frac{-r^2}{4Dt}\right)$$

where D is the diffusion coefficient of the ion which can be obtained from the mean-squared displacement data. Such a fit is shown in Figure 10c, which shows that the transport is very much liquidlike.

We next investigate the dynamics of BO's and NBO's which form part of the network at the same temperatures through the VHS function. We have calculated the VHS of NBO and BO at 1500 K, and they are shown in Figure 11, a and b, respectively. It is evident that there is very little motion of BO's, whereas for the corresponding times NBO's are slightly more mobile. This difference can also be noticed from the diffusion coefficients presented in Table 3. It should be borne in mind that both the species do not show any jumplike features, unlike the K ions. At 2500 K (Figure 12a,b) they are considerably mobile. The behavior obtained from the hydrodynamic equation

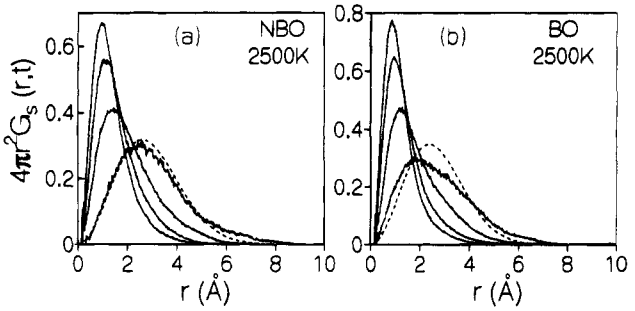

Figure 12. $4\pi r^2G_s(r,t)$ plotted as a function of distance for the NBO and BO ions at 2500 K for various times: (a) NBO and (b) BO. At the first peak position, curves correspond to the following times in decreasing order of height. Time in picoseconds for all cases: 5; 9; 20; 50. The fit of the hydrodynamic diffusion equation for $t = 50$ ps is shown as a dashed line.

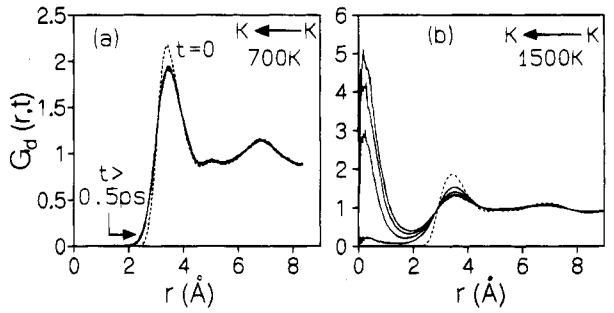

Figure 13. Time-dependent pair correlation function $G_d(r,t)$ for the K−K pair plotted for different times at (a) 700 K and (b) 1500 K. At 700 K, there is almost no change in the function after $t = 0.5$ ps, indicating that K ions are largely immobile. At 1500 K, they migrate by hops to neighboring K ion vacancy sites. In (b), the dashed curve corresponds to $t = 0$, while the other curves correspond to 2, 20, 50, and 80 ps (in the order of increasing height near 0 Å).

for long times is also shown as dashed lines. The data for the NBO fits the equation well while that for BO's is not well described by the equation. This shows that though the glass has melted at 2500 K, a considerable amount of local structure still exists, probably in the form of SiO_4 tetrahedra. Such a notion that liquid alkali silicate retains a large part of its local structure can also be understood from the ΔC_p values at T_g which are generally much smaller (strong liquid) as compared to organic polymers or simple glass forming ionic melts (fragile liquids).[61,62]

Distinct Part of van Hove Correlation Functions. The distinct part of the van Hove correlation function, $G_d(r,t)$ (VHD, also referred to as the time-dependent pair correlation function[55,63]), is an effective tool to understand not only the nature of migration of atoms but also its spatial and temporal dependences. The fact that alkali ions are immobile at 700 K has already been established from the magnitude of MSD and the details of VHS. This observation is also corroborated by the VHD for K−K correlations at 700 K shown in Figure 13a. The first peak height in $G_d(r,t)$ decreases rather fast for very short times and does not relax later for all higher times. The initial fast decay represents vibrational motion (Einstein regime) and the near-constancy of the height of the first peak at later times denotes structural arrest. This behavior is universal to all supercooled liquids below T_g. The most interesting aspect of the migration of K ions can be examined from the behavior of the VHD at 1500 K, where they are reasonably mobile, while the network is largely immobile (Table 3). The VHD function of K ion migration at this temperature allows one to study the specific site to which it migrates. It is reasonable to expect K ions to hop to other K sites in the glass. This is evident from VHD

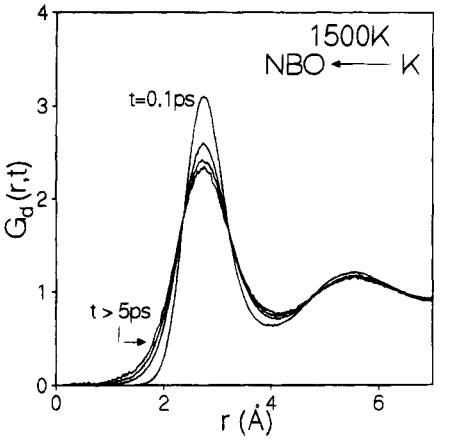

Figure 14. $G_d(r,t)$ function for NBO−K pair at 1500 K for five different times. Since the behavior of the function is almost the same for all times greater than 5 ps, it is concluded that K ions do not migrate to NBO sites.

curves for the probability of potassium to migrate to other potassium sites shown in Figure 13b at 1500 K. From the intensity near 0 Å, it is obvious that K ions hop from their original sites to other K ion sites. For curiosity, VHD functions have also been calculated at 1500 K for K ions to visit NBO sites at future times. This is shown in Figure 14. In all these cases, no peak develops at 0 Å, which shows that K ions migrate only to sites which were previously occupied by other K ions and adds further support to the notion that they maintain their own distinct environments in the glass. In general, site selectivity is a special feature of "strong" glasses where the structural relaxation time (τ_s) and conductivity relaxation time (τ_σ) are quite different.[64] A totally different picture emerges when one studies VHD at a higher temperature, i.e., 2500 K. These are shown for NBO−K and K−K correlations in parts a and b of Figure 15, respectively. The correlation for NBO−K is what one would expect for a liquid.[55] We find that within 50 ps, the correlations have fully died to the uncorrelated value of the function, which is unity. In addition, it should be noted that there are no discernible jump events, as there is no peak at 0 Å at any time, nor is there any minimum in $G_d(r,t)$ between 0 Å and the first-neighbor peak.

This is in sharp contrast to the behavior found for K−K $G_d(r,t)$ at 2500 K shown in Figure 15b. The K−K $G_d(r,t)$ shows that at intermediate times (5 ps and 20 ps in the figure) there seems to be evidence for jumplike behavior. At longer times (40 and 50 ps) the function relaxes fully. This is related to the fact that at any temperature including 2500 K, the network ions are less mobile than the K ions. Hence for times smaller than, say, 20 ps, K ion migration to other K ion vacancies occurs by a jump mechanism, because at these time scales the network ions are still relatively static and hence the identity of a K ion vacancy is very much intact. This identity disappears later, so that the vacancies get "smeared out" by the motion of the network ions, leading to the loss of all correlations in the K−K $G_d(r,t)$. It is also not probably far-fetched to state that, in general, the first step in the transport is an activated hop and that the character of these hops is smeared out at high temperatures and high fluidities. This could result in the well-known diffusive motion characteristic of simple liquids.[65,66] As the temperature is decreased (as in supercooled liquids), activated processes begin to dominate the transport, and at T_g, the long-range diffusion freezes out completely. It is interesting to note, *inter alia*, that the α mode of dielectric relaxation also freezes out.[64] It is widely known that T_g can be defined as that temperature where the time scales of relaxation in a system far

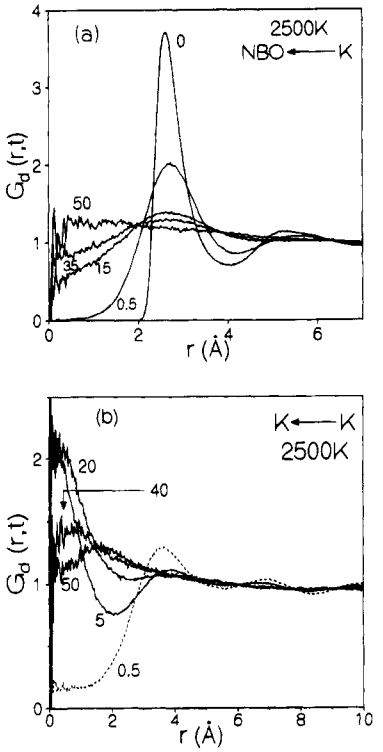

Figure 15. $G_d(r,t)$ curves at 2500 K for (a) the NBO−K pair and (b) the K−K pair for various times (in picoseconds) indicated in the graphs (see the text for details).

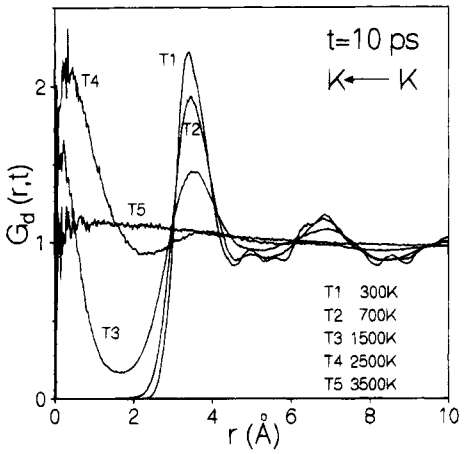

Figure 16. $G_d(r,t)$ function for the K−K pair plotted for five different temperatures, for a time t = 10 ps. There is a qualitative similarity with Figure 15b, indicating time-temperature complementarity.

exceed the experimental time scales. Keeping this in mind, one can easily expect to observe hoplike features in the supercooled liquid regime with high-frequency experimental probes. This is precisely what is observed in the present simulations at smaller times in $G_d(r,t)$. Such a concept was forcefully proposed by Frenkel[67] long ago, that for times smaller than τ, spent by an atom oscillating within a cage (inversely related to its Einstein frequency), a liquid will behave more or less like a solid. Our results provide clear support for this concept.

An even more informative result is shown in Figure 16, where $G_d(r,t)$ curves for K−K correlation are plotted for the five different temperatures for the same time interval of 10 ps. It is transparent that the behavior of $G_d(r,t)$ at various temperatures is identical to those for various time intervals at 2500 K. Such a behavior exemplifies the manifestation of time−temperature complementarity, often exploited in accessing frequency-dependent phenomena by varying the temperature.[64]

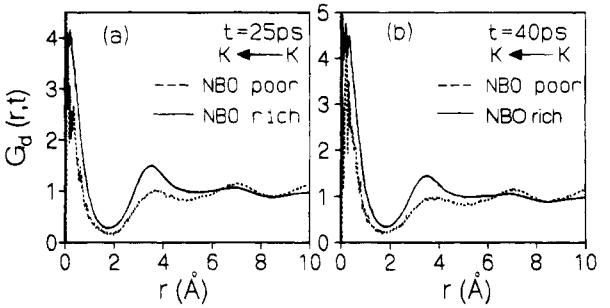

Figure 17. $G_d(r,t)$ function for the K−K pair plotted at 1500 K for the two cases of vacancy sites, NBO poor and NBO rich, at (a) t = 25 ps and (b) t = 40 ps.

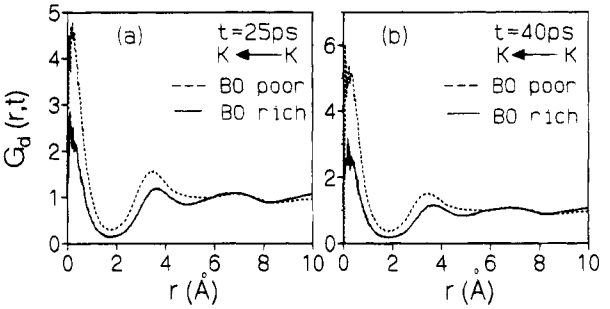

Figure 18. $G_d(r,t)$ function for the K−K pair plotted at 1500 K for the two cases of vacancy sites, BO poor and BO rich, at (a) t = 25 ps and (b) t = 40 ps.

Conduction Pathways. We now focus our attention on the motion of alkali ions at 1500 K, a high enough temperature which is lower than the T_g of the simulated glass. In order to study the detailed migration path of the ions and to see whether there exists any preferred conduction path as proposed by Greaves,[3] we employ two methods. In the first, we use $G_d(r,t)$ itself to find out if there is any preference for K ions to jump to sites rich in NBO. In the second, we directly monitor the motion of individual K ions as they migrate to various sites in the glass and find out the target environment.

In the first method, we divide the 135-ps dynamical data into two sets, each consisting of about 65 ps of data. In a given set of data, we identify sites as either *NBO rich* or *NBO poor*, based on their local environment. A K ion site is defined as *NBO poor* if it is surrounded by two or less NBO's and *NBO rich* if it is surrounded by four or more NBO's. We make this definition at time t = 0 for both the sets of data. Then we calculate the probability for any K ion to migrate to a *NBO poor* site and to a *NBO rich* site. These are given by the respective heights of the 0-Å peak in the $G_d(r,t)$ curve. This is calculated for both the sets of data and the results are combined through time and ensemble averaging. Such a division of the dynamical data into two sets is warranted in this study, as the division of K sites into *NBO rich/poor*, which is made at t = 0, can become invalid at very long times due to the relaxation of the network even at 1500 K. We have observed that the average number of NBO's around K averaged over a 100-ps time interval is around 4.36 with a rms fluctuation of 0.75. Hence such a division of data is essential. The functions for t = 25 ps and t = 40 ps are shown in parts a and b of Figure 17, respectively. It is clear that the probability for K ions to migrate to *NBO rich* sites is larger than that to a *NBO poor* site at both the times. Additional support for this observation comes from a similar set of data for the case of migration to a *BO rich* and *BO poor* site shown in Figure 18 for the same time intervals as in Figure 17. In this case, we find that a predominant number of migrations takes place to *BO poor* sites (which can be

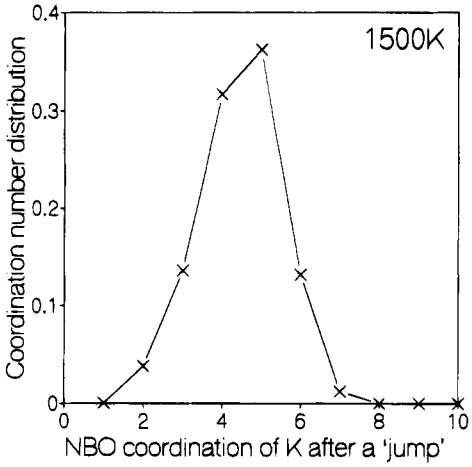

Figure 19. Plot of the NBO coordination number distribution around potassium ions initially present in NBO rich sites immediately after their jumps at 1500 K.

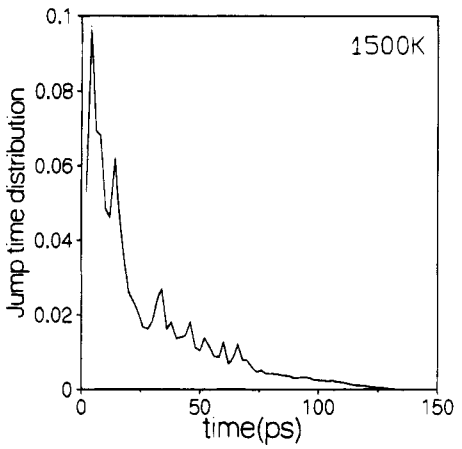

Figure 20. Distribution of the time taken between jumps as a function of time at 1500 K.

considered as *NBO rich*) rather than to a *BO rich* site. It should be cautioned, however, that by this analysis we have not mapped out the existence of NBO rich conduction pathways in the system. What we have attempted to provide is the evidence that K ions largely prefer to migrate to sites which are surrounded by more NBO's than BO's. However, a succession of such preferential migrations of an individual particle can be safely assumed to describe a conduction pathway. It is not very unphysical to visualize the existence of such pathways, at least in the composition which we have studied, namely, the alkali disilicate, because of the high concentration of alkali oxide. A more difficult problem would be to identify the topological dimensionality of the pathway. Various workers including Greaves,[3] Elliott,[68] and Ingram[69] have argued that the pathways are one dimensional. Elliott[68] has made the first clear reference to the dimensionality of conduction pathways, although the "vulnerability" of conductivity to the addition of foreign cations discussed by Ingram[69] implies one-dimensional conduction. The dimensionality of the conduction pathway is also important to explain the mixed-alkali effect in the light of the percolation model of Maass *et al.*[70] However, the present study is not directed to resolve the problem of dimensionality. It only shows that the pathway is actually constituted of NBO rich sites.

That the K ions move largely through NBO rich positions can also be studied directly by monitoring their individual migration in the second method. In this, a given K ion is assumed to have performed a jump if it moves 3.5 Å from its $t = 0$ position (3.5 Å is the K−K nearest-neighbor distance). After each jump, the local environment of each alkali ion is obtained. In defining a jump, care is taken to exclude recrossings. An ion is defined to have recrossed if it is found within a 1-Å radius of one of its previously occupied sites. These recrossings are excluded from the jump statistics. We have then averaged the NBO number distribution around K ions after the jumps. These have been collected only for those ions which are initially *NBO rich*. The distribution is shown in Figure 19, which clearly shows that a predominantly large number of jumps are targetted to NBO rich sites, thus giving additional support to the conduction pathway mechanism of alkali ion transport. Albeit repetitions, we emphasize that both the methods employed in our study to identify the existence of pathways are not free from limitations. The $G_d(r,t)$ method has the problem of the *NBO rich/poor* site losing its identity within the time scales of migration, while in the second method, the definition of a "jump" is somewhat arbitrary. In fact, this problem cannot be resolved clearly. Inherent properties of glass structure (or the lack of it!, namely, the static and dynamic disorder in the system) and dynamics (which is restrictive in the sense that we have to choose temperatures where measurable MSD values of K ions exist, while those of the network ions have to be significantly lower) prevents a sharp definition of jump.[71] Even then, both the results presented so far clearly point toward preferential migration of K ions through NBO rich positions in the glass.

Jump Time Distributions. Activation energies (E_a) for conduction have been calculated by using various models in glassy systems. In general, Coulombic, strain, and polarization energy terms[26,27,72,73] are invoked in order to obtain an estimate of E_a. Until now, E_a has been obtained from MD simulations through the variation of the diffusion coefficient with temperature.[7] In the present study, we employ a simple classical activation picture to obtain E_a. We thus calculate the jump time distributions, i.e., the time between any two jumps. This is shown in Figure 20 at 1500 K. The distribution is rather skewed with a long tail. The first moment of this distribution can be calculated as $\int_0^{t_{max}} tf(t)\,dt$, where $f(t)$ is the jump time distribution. Our studies yield a value of 28 ps for the average jump time. Using this, we can evaluate the activation energy for conduction as $E_a = RT \ln (\nu_0/\nu)$, where ν_0 corresponds to the attempt frequency and can be taken as the cage vibrational frequency of the K ions. ν is the average jump frequency (the inverse of the average jump time), which is 3.5×10^{10} Hz. Thus E_a can be calculated to be 0.62 eV, which agrees very well with the experimental data of the activation energy for conduction (0.6 eV).[10,74]

Various results obtained in the present study have a direct bearing on the present understanding of the mixed-alkali effect (MAE). In an earlier paper,[19] we had observed that the migration of alkali ions in a mixed-alkali silicate glass is preferential and takes place only to like ion sites, due to the large distortion energies needed to accommodate an ion in an unlike ion vacancy site.[75] The temperature dependence of MAE (i.e., the electrical conductivity of the system becoming more linear with the variation of interalkali concentration as temperature is increased) can be easily understood in the light of the present results. At higher temperatures (2500 K), we find that the transport of alkali ions becomes liquid-like, due mainly to the breakdown of the network structure, so much so that K ions in the present study were even observed to visit NBO/BO sites at future times. Thus, there will be no inhibition for K ions to visit alkali ion sites of other type at higher temperatures. In fact, the notion of a distinct "site" itself becomes blurred at these temperatures. Hence the magnitude of MAE will have

to necessarily vanish at some high temperature and thus its dependence on temperature can be understood.

Conclusions

A new partial charge based potential model has been developed and potassium disilicate glass has been investigated. Nonbridging oxygens are treated as distinct entities in this model. The mode is successful in accounting for such subtle effects as a shorter NBO–Si bond in comparison to the BO–Si bond. It is found to provide excellent bond angle distributions, in particular for Si–O–Si. The cage vibrational frequency of potassium ion matches well with experimental results, indicating that the curvature of the potential felt by potassium has been built properly in the potential. The potential is then used to examine the transport mechanism of potassium ions as a function of temperature. K ions migrate by diffusion in the liquid state, whereas in the glassy state their migration occurs by hopping. K ions occupy NBO rich sites and during transport move into other NBO rich sites. Therefore NBO rich conduction pathways appear to be operative during ion transport. The present results give a satisfactory estimate of the activation energy involved in migration also.

Acknowledgment. We thank Prof. C. N. R. Rao, FRS, for his kind encouragement and the Commission of European Communities for financial support.

References and Notes

(1) Zachariasen, W. H. *J. Am. Chem. Soc.* **1932**, *54*, 3841.
(2) Greaves, G. N.; Fontaine, A.; Lagarde, P.; Raoux, D.; Gurman, S. J. *Nature* **1981**, *293*, 611.
(3) Greaves, G. N. *J. Non-Cryst. Solids* **1985**, *71*, 203.
(4) Greaves, G. N.; Gurman, S. J.; Catlow, C. R. A.; Chadwick, A. V.; Houde-Walter, S.; Henderson, C. M. B.; Dobson, B. R. *Philos. Mag. A* **1991**, *64*, 1059.
(5) Ingram, M. D. *Phys. Chem. Glasses* **1987**, *28*, 215.
(6) Elliott, S. R. *Solid State Ionics* **1988**, *27*, 131.
(7) Soules, T. F.; Busbey, R. F. *J. Chem. Phys.* **1981**, *75*, 969.
(8) Angell, C. A.; Boehm, L.; Cheeseman, P. A.; Tamaddon, S. *Solid State Ionics* **1981**, *5*, 597.
(9) Angell, C. A.; Cheeseman, P. A.; Tamaddon, S. *J. Phys.* **1982**, *43*, C9-381.
(10) Abe, Y.; Hosono, H.; Lee, W.-H.; Kasuga, T. *Phys. Rev. B* **1993**, *48*, 15621.
(11) Tsuneyuki, S.; Tsukada, M.; Aoki, H.; Matsui, Y. *Phys. Rev. Lett.* **1988**, *61*, 869. Tsuneyuki, S.; Matsui, Y.; Aoki, H.; Tsukada, M. *Nature* **1989**, *339*, 209. Tsuneyuki, S.; Aoki, H.; Tsukada, M.; Matsui, Y. *Phys. Rev. Lett.* **1990**, *64*, 776.
(12) Rustad, J. R.; Yuen, D. A.; Spera, F. J. *Phys. Rev. A* **1990**, *42*, 2081.
(13) van Beest, B. W. H.; Kramer, G. J.; van Santen, R. A. *Phys. Rev. Lett.* **1990**, *64*, 1955.
(14) Valle, R. G. D.; Andersen, H. C. *J. Chem. Phys.* **1991**, *94*, 5056.
(15) Valle, R. G. D.; Andersen, H. C. *J. Chem. Phys.* **1992**, *97*, 2682.
(16) Somayuzulu, M. S.; Sharma, S. M.; Garg, N.; Chaplot, S. L.; Sikka, S. K. *J. Phys. Cond. Matt.* **1993**, *5*, 6345.
(17) Krol, D. M.; Smets, B. M. J. *Phys. Chem. Glasses* **1984**, *25*, 113.
(18) Alavi, A.; Alvarez, L. J.; Elliott, S. R.; McDonald, I. R. *Philos. Mag. B* **1992**, *65*, 489.
(19) Balasubramanian, S.; Rao, K. J. *J. Phys. Chem.* **1993**, *97*, 8835.
(20) Balasubramanian, S.; Rao, K. J. *J. Non-Cryst. Solids*, in press.
(21) Smets, B. M. J.; Lommen, T. P. A. *J. Non-Cryst. Solids* **1981**, *46*, 21.
(22) Bruckner, R.; Chun, H.-U.; Goretzki, H.; Sammet, M. *J. Non-Cryst. Solids* **1980**, *42*, 49.
(23) Jen, J. S.; Kalinowski, M. R. *J. Non-Cryst. Solids* **1980**, *39*, 21.
(24) Tesar, A. A.; Varshneya, A. K. *J. Chem. Phys.* **1987**, *87*, 2986.
(25) Waseda, Y. *The structure of non-crystalline materials*; McGraw-Hill: New York, 1980.
(26) Rao, K. J.; Estournes, C.; Levasseur, A.; Shastry, M. C. R.; Menetrier, M. *Philos. Mag. B* **1993**, *67*, 389.
(27) Elliott, S. R. *J. Non-Cryst. Solids* **1993**, *160*, 29.
(28) Pant, A. K.; Cruickshank, D. W. J. *Acta Crystallogr. B* **1968**, *24*, 13.
(29) Uchino, T.; Iwasaki, M.; Sakka, T.; Ogata, Y. *J. Phys. Chem.* **1991**, *95*, 5455. Uchino, T.; Sakka, T.; Ogata, Y.; Iwasaki, M. *J. Phys. Chem.* **1992**, *96*, 2455.
(30) Misawa, M.; Price, D. L.; Suzuki, K. *J. Non-Cryst. Solids* **1980**, *37*, 85.
(31) Murdoch, J. B.; Stebbins, J. F.; Carmichael, I. S. E. *Am. Miner.* **1985**, *70*, 332.
(32) Stebbins, J. F. *Nature* **1987**, *330*, 465.
(33) Stebbins, J. F. *J. Non-Cryst. Solids* **1988**, *106*, 359.
(34) Schramm, C. M.; de Jong, B. H. W. S.; Parziale, V. E. *J. Am. Chem. Soc.* **1984**, *106*, 4396.
(35) Dupree, R.; Holland, D.; McMillan, P. W.; Pettifer, R. F. *J. Non-Cryst. Solids* **1984**, *68*, 399. Dupree, R.; Pettifer, R. F. *Nature* **1984**, *308*, 523. Pettifer, R. F.; Dupree, R.; Farnan, I.; Sternberg, U. **1988**, *106*, 408.
(36) Selvaraj, U.; Rao, K. J.; Rao, C. N.R.; Klinowski, J.; Thomas, J. M. *Chem. Phys. Lett.* **1985**, *114*, 24.
(37) Furukawa, T.; Fox, K. E.; White, W. B. *J. Chem. Phys.* **1981**, *75*, 3226.
(38) Greaves, G. N. *Phil. Mag. B* **1989**, *60*, 793.
(39) Vessal, B.; Greaves, G. N.; Marten, P. T.; Chadwick, A. V.; Mole, R.; Houde-Walter, S. *Nature* **1992**, *356*, 504. Elliott, S. R.; *Nature* **1992**, *357*, 650.
(40) Huang, C.; Cormack, A. N. *J. Chem. Phys.* **1991**, *95*, 3634.
(41) Wells, A. F. *Structural Inorganic Chemistry*; Oxford: London, 1975; p 818.
(42) Gaskell, P. H.; Eckersley, M. C.; Barnes, A. C.; Chieux, P. *Nature* **1991**, *350*, 675.
(43) Abramo, M. C.; Caccamo, C.; Pizzimenti, G. *J. Chem. Phys.* **1992**, *96*, 9083.
(44) Farnan, I.; Grandinetti, P. J.; Baltisberger, J. H.; Stebbins, J. F.; Werner, U.; Eastman, M. A.; Pines, A. *Nature* **1992**, *358*, 31.
(45) Soules, T. F. *J. Chem. Phys.* **1979**, *71*, 4570.
(46) Feuston, B. P.; Garofalini, S. H. *J. Chem. Phys.* **1988**, *89*, 5818.
(47) Huang, C.; Cormack, A. N. *J. Chem. Phys.* **1990**, *93*, 8180.
(48) Jin, W.; Vashishta, P.; Kalia, R. K.; Rino, J. P. *Phys. Rev. B* **1993**, *48*, 9359.
(49) Exarhos, G. J.; Risen, W. M., Jr. *Solid State Commun.* **1972**, *11*, 755.
(50) Garofalini, S. H. *J. Chem. Phys.* **1982**, *76*, 3189.
(51) Galeener, F. L.; Leadbetter, A. J.; Stringfellow, M. W. *Phys. Rev. B* **1983**, *27*, 1052.
(52) Price, D. L.; Carpenter, J. M. *J. Non-Cryst. Solids* **1987**, *92*, 153.
(53) Valle, R. G. D.; Venuti, E. *Chem. Phys.* **1994**, *179*, 411.
(54) Zdaniewski, W. A.; Rindone, G. E.; Day, D. E. *J. Mat. Sci.* **1979**, *14*, 763.
(55) Hansen, J.-P.; McDonald, I. R. *Theory of simple liquids*; Academic: London, 1986.
(56) Roux, J.-N.; Barrat, J.-L.; Hansen, J.-P. *J. Phys. Condes. Matter.* **1989**, *1*, 7171.
(57) Barrat, J.-L.; Roux, J.-N.; Hansen, J.-P. *Chem. Phys.* **1990**, *149*, 197.
(58) Barrat, J.-L.; Klein, M. L. *Annu. Rev. Phys. Chem.* **1991**, *42*, 23.
(59) Wahnström, G. *Phys. Rev. A* **1991**, *44*, 3752.
(60) Bohmer, R.; Gerhard, G.; Drexler, F.; Loidl, A.; Ngai, K. L.; Pannhorst, W. *J. Non-Cryst. Solids* **1993**, *155*, 189.
(61) Angell, C. A. *J. Phys. Chem. Solids* **1988**, *49*, 863.
(62) Bohmer, R.; Ngai, K. L.; Angell, C. A.; Plazek, D. J. *J. Chem. Phys.* **1993**, *99*, 4201.
(63) Rahman, A. *Phys. Rev. A* **1964**, *136*, 405.
(64) Angell, C. A. *Chem. Rev.* **1990**, *90*, 523.
(65) Seeley, G.; Keyes, T. *J. Chem. Phys.* **1989**, *91*, 5581.
(66) Stillinger, F. H.; Weber, T. A. *J. Chem. Phys.* **1984**, *80*, 4434.
(67) Frenkel, J. *Kinetic theory of liquids*; Dover: New York, 1955, p 188.
(68) Elliott, S. R.; Owens, A. P. *Philos. Mag. B* **1989**, *60*, 777.
(69) Ingram, M. D. *Phil. Mag. B* **1989**, *60*, 729.
(70) Maass, P.; Bunde, A.; Ingram, M. D. *Phys. Rev. Lett.* **1992**, *68*, 3064.
(71) Nitzan, A.; Ratner, M. A. *J. Phys. Chem.* **1994**, *98*, 1765.
(72) Anderson, O. L.; Stuart, D. A. *J. Am. Cer. Soc.* **1954**, *37*, 573.
(73) Martin, S. W.; Angell, C. A. *J. Non-Cryst. Solids* **1986**, *83*, 185.
(74) Charles, R. J. *J. Am. Cer. Soc.* **1966**, *49*, 55. Frischat, G. H. *Ionic Diffusion in Oxide Glasses*; Trans Tech: Aedermannsdorf, 1975.
(75) Uchino, T.; Sakka, T.; Ogata, Y.; Iwasaki, M. *J. Non-Cryst. Solids* **1992**, *146*, 26.